J|A|C|S
ARTICLES
Published on Web 05/18/2002

Large-Scale Resonance Amplification of Optical Sensing of Volatile Compounds with Chemoresponsive Visible-Region Diffraction Gratings

Ryan C. Bailey and Joseph T. Hupp*

Contribution from the Department of Chemistry, Materials Research Center and Center for Nanofabrication and Molecular Self-Assembly, Northwestern University, Evanston, Illinois 60208

Received December 11, 2001

Abstract: Micropatterning of the vapochromic charge-transfer salt, $[Pt(CNC_6H_4C_{10}H_{21})_4][Pd(CN)_4]$, on transparent platforms yields transmissive chemoresponsive diffraction gratings. Exposure of the gratings to volatile organic compounds (VOCs) such as chloroform and methanol leads to VOC uptake by the porous material comprising the grating lattice or framework, and a change in the material's complex refractive index, $\tilde{n}$. The index change is accompanied by a change in the degree of index contrast between the lattice and the surrounding medium (in this case, air), and a change in the diffraction efficiency of the grating. When a monochromatic light source that is not absorbed by the lattice material is employed as a probe beam, only changes in the real component of $\tilde{n}$ are sensed. Under these conditions, the grating behaves as a nonselective, but moderately sensitive, sensor for those VOCs capable of permeating the porous lattice material. When a probe color is shifted to a wavelength coincident with the vapochromic charge-transfer transition of the lattice material, the sensor response is selectively amplified by up to 3.5 orders of magnitude, resulting in greatly enhanced sensitivity and some degree of chemical specificity. On the basis of studies at four probe wavelengths, the amplification effect is dominated by resonant changes in the imaginary component of the refractive index. The observed wavelength- and analyte-dependent amplification effects are quantitatively well described by a model that combines a Kramers−Kronig analysis with an effective-medium treatment of dielectric effects.

Introduction

Two distinct subproblems comprise nearly all chemical and biochemical sensing problems: (1) recognition and binding of the ion or molecule to be sensed, and (2) transduction of the recognition/binding event into an externally observable signal. Recently, we described a conceptually new approach to the second subproblem − signal transduction.[1] Briefly, using soft lithography techniques, we constructed transmissive 2-D gratings or "photonic lattices" of materials featuring nanoscale porosity and significant affinities for the molecules or ions targeted for sensing. With a lattice periodicity of ca. 10 μm, these gratings readily diffract monochromatic visible light, yielding a characteristic diffraction pattern that is related to the physical pattern of the lattice by a Fourier transform; see Scheme 1. The efficiency of diffraction, that is, the ratio of diffracted light intensity to total transmitted light intensity, depends in part on the degree of refractive index contrast ($\Delta\tilde{n}$) between the lattice material and the surrounding medium (typically air or water for environmental sensing applications). Uptake of polarizable analyte species by the nanoscale-void-containing lattice material causes the refractive index of the lattice to increase, since the air (essentially vacuum, $n \approx 1$) or water ($n = 1.33$) initially occupying the void space is replaced, for example, by an organic analyte featuring a refractive index of ∼1.4−1.5. The increased index for the porous lattice (a composite of sorptive material, analyte species, and air or water) yields a greater degree of index contrast with the surrounding medium, and an increase in diffraction efficiency.[2] The change in diffraction efficiency is readily monitored with a pair of photodiodes.

Scheme 1. Illustration of the Experimental Setup

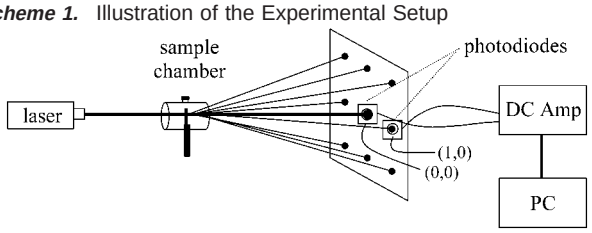

* To whom correspondence should be addressed. E-mail: jthupp@chem.nwu.edu.

(1) Mines, G. A.; Tzeng, B.; Stevenson, K. J.; Li, J.; Hupp, J. T. *Angew. Chem., Int. Ed.* **2002**, *41*, 154−157.

(2) For other examples of chemically modulated film-based diffraction unrelated to sensing, see: (a) Bergstedt, T. S.; Hauser, B. T.; Schanze, K. S. *J. Am. Chem. Soc.* **1994**, *116*, 8380. (b) Hauser, B. T.; Bergstedt, T. S.; Shanze, K. S. *J. Chem. Soc., Chem. Commun.* **1995**, 1945−1946. (c) Wu, Y.; Pfennig, B. W.; Bocarsly, A. B.; Vicenzi, E. P. *Inorg. Chem.* **1995**, *34*, 4262−4267. (d) Bocarsly, A. B.; Chang, C. C.; Wu, Y.; Vicenzi, E. P. *J. Chem. Educ.* **1997**, *74*, 663−667. (e) Massari, A. M.; Stevenson, K. J.; Hupp, J. T. *J. Electroanal. Chem.* **2001**, *500*, 185−191. (f) Dang, X.; Massari, A. M.; Hupp, J. T. *Electrochem. Solid-State Lett.* **2000**, *3*, 555−558. (g) Zettsu, N.; Ubukata, T.; Seki, T.; Ichimura, K. *Adv. Mater.* **2001**, *13*, 1693−1697.

Initial studies focused on proof-of-concept detection of uptake of (a) chloroform and trichlorophenol by porous titanium dioxide lattices,[3] (b) pyridine, dioxane, and benzene by lattices of porphyrinic "molecular square" materials,[2] and (c) Zn^{2+} and molecular iodine by receptor-functionalized "molecular square" materials.[1] Using quartz crystal microgravimetry (QCM) for validation, excellent correspondence was obtained between the magnitude of the signal (i.e., change in diffraction efficiency, ΔDE) and the amount of analyte taken up. Good, but not outstanding, sensitivity was observed. For example, for TiO_2 lattices, the sensitivity was about 1 order of magnitude less than that observed with QCM for comparable films under equivalent conditions. Like QCM, the photonic lattice sensing modality is essentially universal with respect to analyte identity: all molecules contain polarizable electrons. Therefore, all molecules are capable, in principle, of inducing refractive index changes and altering diffraction efficiencies given appropriate porous host materials. While this renders the technique attractive (since special signal transduction properties such as fluorescence or redox reactivity need not be tagged to the analytes or engineered into the chemosensory materials), it also represents a drawback in that chemical selectivity, at the transduction stage, is sacrificed. Similar conclusions can be drawn for other sensing schemes which rely upon changes in refractive index for signal transduction.[5] Examples of these include chemically sensitive optical fibers and waveguides,[6−8] thin-film interferometry from porous silicon,[9,10] Bragg-reflector-based porous silicon mirocavities,[11] Kretschmann geometry surface plasmon resonance (SPR) spectroscopy,[12,13] and localized surface plasmon (LSPR) spectroscopy.[14,15]

We reasoned that by making measurements under conditions of electronic resonance, that is, conditions where the lattice material absorbs probe light, the diffraction efficiency could be greatly amplified, and detection limits for photonic-lattice-based chemical sensing could be significantly extended. We further reasoned that the resonance amplification phenomenon could be exploited to impart chemical selectivity to the signal transduction process. To test these ideas, we have employed a porous "vapochromic" charge-transfer compound as a lattice material. Mann and co-workers have previously shown how the absorption and/or luminescence of these compounds can be used to sense an impressive range of volatile organic compounds at saturation vapor pressures.[16,17] By exploiting the vapochromic behavior in a resonance sense, we find that photonic lattice responses to a representative analyte, chloroform, can be amplified by 3.5 orders of magnitude. We additionally find that the amplification can be engendered selectively; under non-resonance conditions, chloroform and methanol are both detected with similarly low sensitivity. However, under resonance conditions, signals for chloroform vapor are strongly preferentially amplified. The combined findings comprise tremendous improvements in the sensitivity and selectivity of the new signal transduction modality, and suggest real utility for the approach in the context of chemical sensing.

We present below the details of the new experiments as well as the results of computational modeling studies. We find that the remarkable amplification effects can be described in a quantitative fashion via a combination of Kramers−Kronig theory and effective-medium theory. We suggest that the theory and associated modeling can ultimately be employed in a predictive fashion for the discovery and development of new lattice-based chemical and biochemical sensors.

Experimental Section

Preparation of Micropatterned $[Pt(CNC_6H_4C_{10}H_{21})_4][Pd(CN)_4]$ Films. The vapochromic charge-transfer salt $[Pt(CNC_6H_4C_{10}H_{21})_4][Pd(CN)_4]$ was synthesized according to previous reports[16] and stored under vacuum until use. Because of the low solubility of the material, films were cast from a hexane suspension (∼1 mg in ∼10 mL). The material was micropatterned via the micromolding in capillaries (MIMIC)[18] technique. Briefly, a patterned poly(dimethylsiloxane) (PDMS) stamp having an array of 5×5 μm^2 square features with a periodicity of 10 μm was fabricated by a previously reported procedure.[19] The stamp was brought into contact with a clean glass microscope slide, and a small weight (∼10 g/cm^2) was placed on top to ensure uniform contact. A small drop of the suspended material was then placed beside the stamp and drawn into the pattern via capillary action. After allowing the solvent to evaporate, the PDMS stamp was removed, revealing the micropatterned film.

Characterization of Micropatterned $[Pt(CNC_6H_4C_{10}H_{21})_4][Pd(CN)_4]$ Films. Visible-region extinction measurements were made with a HP-8452A diode array spectrophotometer. Surface topographical characterization was performed using a Digital Instruments Multimode Nanoscope IIIa atomic force microscope operating in tapping mode (cantilever length 125 μm and resonance frequency 307−367 Hz, Digital Instruments).

Diffraction Measurements. A schematic of the instrumentation used in diffraction experiments is shown in Scheme 1. The light sources utilized in the measurements were helium−neon gas lasers ($\lambda = 632.8$ nm, JDS Uniphase and $\lambda = 543.5$ nm, Melles-Griot), a tunable dye laser (Spectra Physics), and a near-IR diode laser (Liconix DioLite Model 8000). The film was placed in an airtight 300 mL quartz cell so that the incident laser radiation was normal to the sample. The volatile organic analyte was injected through a nonabsorbing silicone/PTFE septum. Diffracted ($I_{1,0}$) and undiffracted ($I_{0,0}$) beams were collected using silicon photodiodes, generally at a rate of 1 Hz. Diode signals were first amplified as needed by a home-built DC amplifier, and then digitized by a personal computer via Lab View software (National Instruments Corp., Austin, TX). Data treatment typically included performing a 25-point floating average on the raw diode voltage output, followed by dividing $I_{1,0}$ by $I_{0,0}$ to obtain an operational "diffraction efficiency"; see below.

(3) Dang, X.; Stevenson, K. J.; Hupp, J. T. *Langmuir* **2001**, *17*, 3109−3112.
(4) Reference deleted in press.
(5) Janata, J.; Josowicz, M.; Vanysek, P.; DeVaney, D. M. *Anal. Chem.* **1998**, *70*, 179R−208R.
(6) *Chemical and Biochemical Sensing with Optical Fibers and Waveguides*; Artech House: Norwood, MA, 1996.
(7) Kooyman, R. P. H.; Lechuga, L. M. *Handbook of Biosensors and Electronic Noses*; CRC Press: Boca Raton, FL, 1997.
(8) Lenferink, A. T. M.; Schipper, E. F.; Kooyman, R. P. H. *Rev. Sci. Instrum.* **1997**, *68*, 1582−1586.
(9) Gao, J.; Gao, T.; Li, Y. Y.; Sailor, M. J. *Langmuir* **2002**, *18*, 2229−2233.
(10) Dancil, K.-P. S.; Greiner, D. P.; Sailor, M. J. *J. Am. Chem. Soc.* **1999**, *121*, 7925−7930.
(11) Chan, S.; Homer, S. R.; Fauchet, P. M.; Miller, B. L. *J. Am. Chem. Soc.* **2001**, *123*, 11797−11798.
(12) Grassi, J. H.; Georgiadis, R. M. *Anal. Chem.* **1999**, *71*, 4392−4396.
(13) Jordan, C. E.; Frutos, A. G.; Thiel, A. J.; Corn, R. M. *Anal. Chem.* **1997**, *69*, 4939−4947.
(14) Malinsky, M. D.; Kelly, K. L.; Schatz, G. C.; Van Duyne, R. P. *J. Phys. Chem. B* **2001**, *105*, 2343−2350.
(15) Selectivity, of course, can always be introduced at the analyte recognition stage if an appropriate receptor molecule can be incorporated, as elegantly shown, for example, by Dancil et al. (ref 9) and Chan et al. (ref 10) in their studies of interferometry-based biosensing.
(16) Exstrom, C. L.; Sowa, J. R.; Daws, C. A.; Janzen, D.; Mann, K. R. *Chem. Mater.* **1995**, *7*, 15−17.
(17) Daws, C. A.; Exstrom, C. L.; Sowa, J. R.; Mann, K. R. *Chem. Mater.* **1997**, *9*, 363−368.
(18) Xia, Y.; Whitesides, G. M. *Angew. Chem., Int. Ed. Engl.* **1998**, *37*, 550−575.
(19) Stevenson, K. J.; Hurtt, G. J.; Hupp, J. T. *Electrochem. Solid-State Lett.* **1999**, *2*, 175−177.

Theory and Modeling

Background Diffraction Theory. Diffraction occurs when coherent radiation encounters a spatially periodic contrast of the complex index of refraction, $\tilde{n}$. The index can be written as a sum of real (n) and imaginary (k) components:

$$\tilde{n} = n + ik \tag{1}$$

The two components vary spatially and are wavelength dependent. The imaginary component of the index is related to the wavelength-dependent absorbance ($A(\lambda)$) by[20]

$$k(\lambda) = \frac{2.3\lambda A(\lambda)}{4\pi d} \tag{2}$$

where d is the grating thickness, and λ is the wavelength. A periodic contrast of *either* component of the refractive index will result in diffraction. Modulation of n results in phase grating behavior, and contrast of k results in amplitude grating behavior. If both n and k are modulated, then the resulting grating is classified as a mixed grating. Under nonresonant conditions, the lattices exhibit pure phase grating behavior. However, under resonance conditions, the lattices behave as mixed gratings, requiring treatment of both n and k to properly address the chemosensing problems examined here.

For a lossless grating, the efficiency, η, with which light is partitioned into each diffracted spot is defined as the ratio of the light intensity at the spot to the total incident intensity. This efficiency can be expressed in terms of the amplitude functions of the respective diffraction order and the incident plane wave of light:

$$\eta_m = \frac{I_m}{I_i} = \left|\frac{A_m}{A_i}\right|^2 \tag{3}$$

where I_m and I_i are the intensities of the m^{th} order diffracted spot and incident beam, respectively, and A_m and A_i are the corresponding amplitude functions.[21]

Neglecting reflective losses, the amplitude function for the m^{th} order diffracted spot can be calculated by integrating the normalized transmission function for the grating over the grating periodicity.[21] The extension of this theory to two dimensions was accomplished by first defining the pattern in terms of the 2-D indexes h and j, and then integrating over both periodicity directions, as shown below:

$$\sqrt{\eta_{h,j}} = \left|\left(\frac{1}{\Lambda_x\Lambda_y}\right)\int_0^{\Lambda_x}\int_0^{\Lambda_y} t(x,y)\,\exp\left[i\left(\frac{h2\pi x}{\Lambda_x} + \frac{j2\pi y}{\Lambda_y}\right)\right]\mathrm{d}x\mathrm{d}y\right| \tag{4}$$

In eq 4, which assumes normal incidence, $\eta_{h,j}$ is the diffraction efficiency of spot (h,j), Λ_x and Λ_y are the x and y periodicities, respectively, $t(x,y)$ is the two-dimensional transmission function, and d signifies a differential, not a thickness. In regions where no grating material is present, the transmission function of a grating is defined as $t(x,y) = 1$, while for areas where grating material exists:[22]

$$t(x,y) = e^{i\phi} \tag{5a}$$

(20) Schanze, K. S.; Bergstedt, T. S.; Hauser, B. T.; Cavalaheiro, C. S. P. *Langmuir* **2000**, *16*, 795−810.

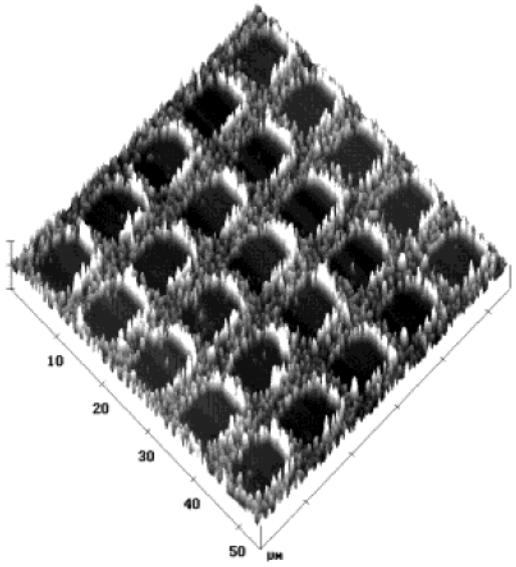

Figure 1. Tapping mode AFM image of a portion of a representative micropatterned vapochromic lattice. The average film thickness was measured to be 69 ± 5 nm.

where

$$\phi = \frac{2\pi\Delta\tilde{n}d}{\lambda} \tag{5b}$$

For this particular lattice geometry, it is mathematically convenient that the gratings employed in the diffraction experiments have a periodicity of 10 μm in each direction (x and y) and that the patterned square vacancies have dimensions of 5 × 5 μm^2. This permits eq 4 to be approximated with the following simplified expression:[23]

$$\eta_{1,0} = 0.0253\,\sin^2(\phi) \tag{6}$$

A further approximation, which is valid in the thin-film limit, is[24]

$$\eta_{1,0} = 0.1012\left(\frac{\pi d}{\lambda\cos\theta}\right)^2[(\Delta n)^2 - (\Delta k)^2] \tag{7}$$

Results and Discussion

Micropatterned Film Characterization. The micropatterned structure of the $[Pt(CNC_6H_4C_{10}H_{21})_4][Pd(CN)_4]$ vapochromic thin film was verified by atomic force microscopy. Multiple large area scans (data not shown) revealed that the micropattern is continuous over a very sizable area (~4 mm^2). A smaller 55 × 55 μm^2 image is shown in Figure 1. The average lattice thickness was measured to be 69 ± 5 nm. As evidenced by the micrograph, the inverted pattern of the stamp is extremely well replicated, and the empty 5 × 5 μm^2 wells are well defined with respect to the surrounding material. The observed microstructure is likely indicative of microcrystallinity.[16]

Shown in Figure 2 is an absorption spectrum of a "thick" film (~300 nm; no micropatterning) of $[Pt(CNC_6H_4C_{10}H_{21})_4]$-

(21) Eichler, H. J.; Gunter, P.; Pohl, D. W. *Laser-Induced Dynamic Gratings*; Springer-Verlag: New York, 1986; Vol. 50.
(22) Grzybowski, B. A.; Qin, D.; Whitesides, G. M. *Appl. Opt.* **1999**, *38*, 2997−3002.
(23) Magnusson, R.; Gaylord, T. K. *J. Opt. Soc. Am.* **1978**, *68*, 806−809.
(24) Nelson, K. A.; Casalegno, R.; Miller, R. J. D.; Fayer, M. D. *J. Chem. Phys.* **1982**, *77*, 1144.

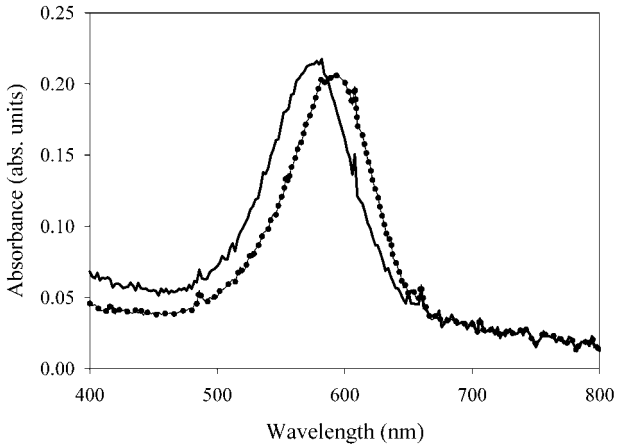

Figure 2. Visible region absorption spectra of a $[Pt(CNC_6H_4C_{10}H_{21})_4][Pd(CN)_4]$ film before and after addition of $CHCl_3$, demonstrating the vapochromic nature of the material. The absorption maximum shifts from 578 to 592 nm.

$[Pd(CN)_4]$ obtained before and after exposure to a chloroform saturated air environment.[25] The observed absorption, which has previously been assigned to a metal(platinum)-to-ligand charge transfer (MLCT) transition, shifts from $\lambda_{max} = 578$ nm to $\lambda_{max} = 592$ nm. Mann and co-workers have postulated several mechanisms by which this "vapochromic" behavior may be induced.[16,17,26,27] Absorption spectra measured for $[Pt(CNC_6H_4C_{10}H_{21})_4][Pd(CN)_4]$ in the presence of analyte-free, chloroform-saturated, and methanol-saturated air were found to display maxima that were reproducibly red-shifted by 14 nm from those reported in the literature.[16] These differences are not completely understood; however, they may in part reflect a sensitivity to UV−vis collection methodology and angle of incidence.[28] To best match the conditions of the diffraction experiment conditions (see below), the absorption spectra were collected at normal incidence.

Notably, other intercalants induce different red shifts or, in a few cases, slight blue shifts.[16] Methanol uptake, for example, induces a 6 nm blue shift.

Chemoresponsive Resonant and Nonresonant Diffraction Behavior. A digital image of a representative diffraction pattern from a micropatterned thin film of the charge-transfer compound is shown in Figure 3. The observed response can be used to define a loss-corrected diffraction efficiency at one of the first-order spots:

$$DE_{1,0} = \frac{I_{1,0}}{I_{total}} \approx \frac{I_{1,0}}{I_{0,0}} \qquad (8)$$

In the equation, I_{total} is the total transmitted light intensity, and $I_{1,0}$ and $I_{0,0}$ are the intensities of one of the first-order diffraction beams and the undiffracted beam, respectively; see Figure 3. The loss correction, which even under resonance conditions amounts to only a few percent here, is inherent to the substitution of the transmitted intensity for the incident intensity. In addition, the comparatively weak diffraction displayed by these very short path length lattices permits I_{total} to be approximated by $I_{0,0}$ with negligible loss of accuracy.

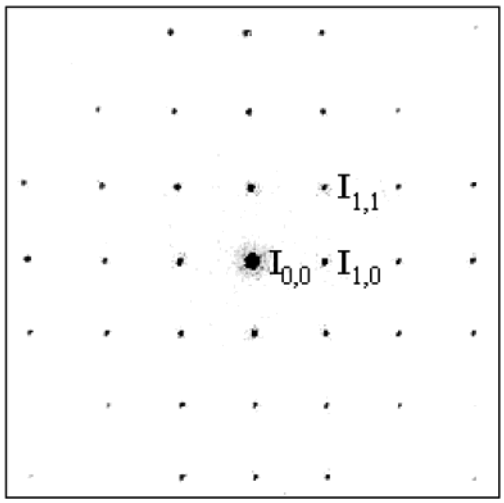

Figure 3. Digital image of the diffraction pattern generated by passing a He−Ne laser beam ($\lambda = 632.8$ nm) through the micropatterned lattice.

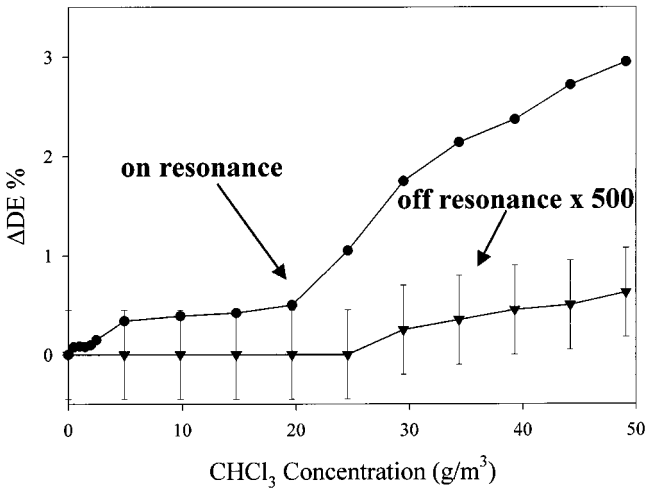

Figure 4. Uptake isotherms for chloroform measured at resonant (−●− 632.8 nm) and nonresonant (−▼− 834 nm) wavelengths. Note that the response at 834 nm has been multiplied by 500 to facilitate comparisons. The signals measured at 632.8 nm are about 3000 times larger than those measured at 834 nm.

Sensing experiments were initially run under nonresonant conditions, that is, at a wavelength (834 nm) where the lattice does not absorb. Exposure of the lattice to varying vapor pressures of chloroform yielded the lower curve shown in Figure 4.[29] As expected for replacement of air or vacuum by chloroform within the porous lattice material, the diffraction efficiency increases slightly. To test the notion of resonance enhancement, we extended the study to a probe wavelength, λ_P, of 632.8 nm where the lattice absorbs (see Figure 2). We found that the change in $DE_{1,0}$ due to chloroform uptake is very substantially enhanced, ca. 3000-fold greater than found away from resonance; see upper curve in Figure 4.[30] At a $CHCl_3$ vapor pressure of 49 g/m^3 (the highest concentration examined), this corresponds to a normalized percentage change in $DE_{1,0}$ of 2.95. (In other words, $DE_{1,0}$(49 g/m^3)/$DE_{1,0}$(0 g/m^3) = 1.0295.)

(25) A spectrum of a "thick" film is shown because of limited instrument resolution when analyzing weakly absorbing (OD < 0.02) specimens.
(26) Buss, C. E.; Mann, K. R. *J. Am. Chem. Soc.* **2002**, *124*, 1031−1039.
(27) Buss, C. E.; Anderson, C. E.; Pomije, M. K.; Lutz, C. M.; Britton, D.; Mann, K. R. *J. Am. Chem. Soc.* **1998**, *120*, 7783−7790.
(28) Mann, K. R., personal communication.
(29) To obtain data off resonance at 834 nm, we found it necessary to average 120 000 points at each concentration (100 point/s × 1200 s).

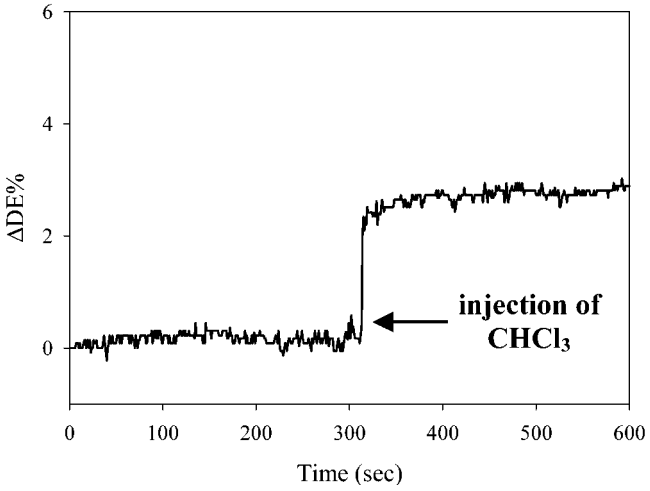

Figure 5. Typical time-resolved diffraction experiment at 632.8 nm, in which $CHCl_3$ was injected into an airtight chamber containing the vapochromic diffraction grating to give a concentration of 49 g/m^3. Injection occurred at $t = 300$ s. No data averaging or curve smoothing was employed.

Extension of the measurement to $\lambda_P = 543.5$ nm yielded a 650-fold enhancement or amplification of the nonresonant $\Delta DE_{1,0}$ response. Measurements at $\lambda_P = 578$ nm also yielded a highly amplified response (~4000 times the nonresonant $\Delta DE_{1,0}$ value), but opposite in sign to other measurements; that is, the diffraction efficiency *decreased* upon uptake of the analyte. At a $CHCl_3$ vapor pressure of 49 g/m^3, the amplification factors at 543.5 and 578 nm translate into normalized diffraction efficiency changes of 0.79 and −3.34%, respectively.

In addition to signal magnitude, signal time response is of interest. Figure 5 shows a representative time-resolved response upon injection of chloroform. The response is reasonably rapid, consistent with reports by Mann and co-workers[16,17] based on absorption, luminescence, and quartz crystal microgravimetry.

Chemical Selectivity. As discussed in previous reports on $[Pt(CNC_6H_4C_{10}H_{21})_4][Pd(CN)_4]$, the magnitude and direction of the observed absorbance shift vary with the identity of the analyte.[16] Because of this, we reasoned that the analyte-specific vapochromic shift, that is, analyte-specific resonance condition, might impart some chemical selectivity to the resonant diffraction-based sensing scheme. This was tested by monitoring the change in diffraction efficiency of the vapochromic lattice in response to exposure to each of two analytes (chloroform and methanol) at a single wavelength (632.8 nm). As illustrated in Figure 2, the chloroform-saturated lattice absorbs significantly at $\lambda_p = 632.8$ nm, and hence shows a resonantly enhanced diffraction response (see above text and Figure 4). In contrast, the absorption maximum of the material blue-shifts by 6 nm upon exposure to methanol (data not shown), so that 632.8 nm is less strongly resonant with the electronic transition. An experiment analogous to that shown in Figure 5 was performed with the lattice exposed to 27 g/m^3 of methanol vapor. Under these nonresonant conditions, the response was observed to be very small, $<0.1\%$ ΔDE.

Kramers−Kronig Modeling. As noted above, phase grating behavior arises from spatially periodic fluctuations in the real component of the refractive index. In the vicinity of an absorption band (an imaginary component of the refractive index), the real component can vary significantly, depending on the wavelength, both increasing and decreasing with respect to nonresonant values. The effects can be quantified, in part, via the Kramers−Kronig relationship[20] (eq 9) which succinctly describes how wavelength-dependent differences in absorption coefficient, ($\Delta\alpha$),[31] between the lattice and surrounding medium (in this case, air), influence the real component of the refractive index:

$$\Delta n(\omega') = \frac{c}{\pi}\int_0^\infty \frac{\Delta\alpha(\omega)}{\omega^2 - \omega'^2}\,d\omega \qquad (9)$$

In the equation, c is the speed of light, λ is the incident wavelength, ω is the angular frequency ($2\pi c/\lambda$), and $\Delta n(\omega')$ is the change in the real component of the refractive index at angular frequency ω'.

To model the resonant diffraction response of the lattice to chloroform uptake, we first used eq 9 to calculate Δn as a function of wavelength, in the presence and in the absence of chloroform. These results were then employed in both the exact (eq 6) and the approximate (eq 7) expressions to generate wavelength-dependent efficiencies, first in the absence and then in the presence of chloroform. Their difference, that is, the calculated *change* in DE due to $CHCl_3$ uptake, is shown versus wavelength in Figure 6a.

It is evident that the Kramers−Kronig analysis captures, in part, the wavelength-dependent enhancement of ΔDE observed experimentally. For example, it yields an increase in diffraction efficiency at 632.8 nm and a decrease in DE at 578 nm. In contrast, however, to the experimental observation of roughly equal absolute changes in *DE* at the two wavelengths, the analysis promises a large change at 578 nm and a much smaller change at 632.8 nm. Additionally, at 543.5 nm it promises a modest decrease in *DE*, whereas a small increase is observed experimentally.

In view of the small absorbance changes involved ($\Delta A(\max) < 0.02$), we initially suspected that amplitude contributions to the *change* in DE would be negligible. However, to account for the above-mentioned discrepancies, we set out to elucidate the effect of the absorbance shift (amplitude grating) on the change in diffraction efficiency. For the sake of comparison, the change in diffraction efficiency was calculated using eq 6 considering only imaginary component (Δk) contributions and compared to the real component contributions (as shown in Figure 6a). This comparison is shown graphically in panel b of Figure 6. Notably, despite the fact that the overall diffraction process is dominated by phase grating effects, the calculated *change* in diffraction efficiency is dominated by amplitude grating behavior, with only minor contributions from phase grating behavior.

(30) Although the resonant (632.8 nm) and nonresonant (834 nm) isotherms appear to be similarly shaped, implying similar amplification at different analyte concentrations, the signal-to-noise ratio at 834 nm is too poor to determine whether the degree of amplification indeed is concentration independent. If the changes in lattice absorption induced by analyte uptake correspond to loss of one chromophoric form and formation of only one other, rather than formation of a series of progressively more highly solvated chromophores, the amplification factor is anticipated to be concentration independent. On the other hand, if more than one form of the solvated chromophore exists, the amplification factor will vary. We do not know which description is more accurate here. Mann has shown that some systems display a single isosbestic point (see refs 15, 16), while others show two isosbestic points (see refs 25, 26) in visible-region spectral measurements and X-ray diffraction techniques.

(31) $\alpha = 2.303A(\lambda)/T$.

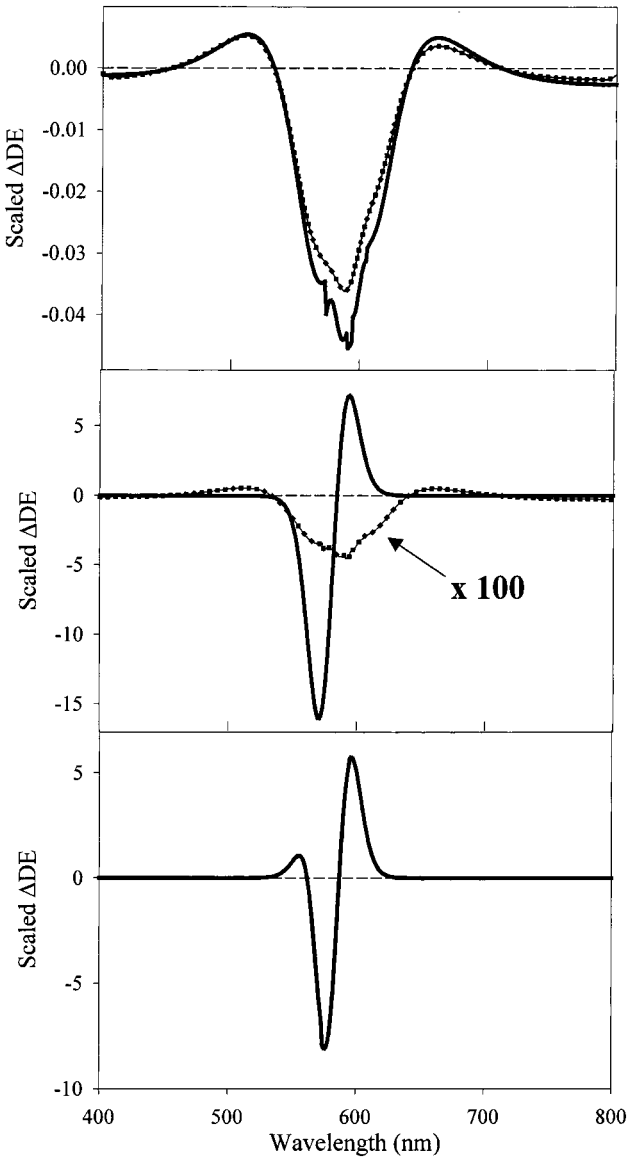

Figure 6. Wavelength-dependent diffraction response upon chloroform addition described by (a) treatment of Δn only by implementing eq 6 (−) and eq 7 (−■−), (b) separate treatment of Δn (−■−) and Δk (−) by eq 6, illustrating the amplitude and phase contributions to the change in diffraction efficiency, and (c) combined treatment by consideration of $\Delta(n + ik)$ by eq 6.

With these calculations in hand, we calculated the wavelength-dependent *change* in *DE* when considering both real and imaginary components of the refractive index [$\Delta(n + ik)$]. The outcome of that calculation is shown in panel c of Figure 6. While the full consideration of both amplitude and phase effects obviously provides significant improvement, discrepancies still exist between experimental and calculated data. One factor not yet considered is that the incorporated analyte possesses a refractive index greater than that of the initially vacant void region of the porous host. This issue is addressed in the following section.

Effective-Medium Modeling. Kramers−Kronig modeling takes into account the effect of wavelength-dependent absorption coefficient changes (imaginary refractive index changes) upon the real component of the refractive index and the loss-corrected diffraction efficiency. The Kramers−Kronig analysis does not consider, however, the origin of the absorption coefficient changes. For example, thermochromic effects would be treated in exactly the same fashion as vapochromic or solvatochromic effects, even though the latter involve the uptake of analyte molecules and a change, therefore, in the local dielectric environment of the chromophoric entities comprising the lattice. It is this change in local dielectric and, in turn, the average dielectric of the porous lattice that largely accounts for the differential diffraction response observed under nonresonant conditions (Figure 4, lower curve).

Under resonance conditions, the consequences of altering the dielectric environment by absorbing analyte molecules are more complicated, and a simple volume-weighted combination of the dielectric properties of the analyte and initially empty lattice is insufficient to describe the altered diffraction behavior. Effective-medium theory would be more appropriate. Recalling that the refractive index is the square root of the dielectric function, an effective-medium approximation can be used to estimate the contributions of the analyte to the overall complex refractive index. A useful effective-medium approximation, known as Maxwell−Garnett theory,[32] treats analyte molecules simply as spherical inclusions within a bulk material matrix, and is the following:

$$\frac{\epsilon_{\text{eff}} - \epsilon_{\text{mat}}}{\epsilon_{\text{eff}} - 2\epsilon_{\text{mat}}} = f\frac{\epsilon_{\text{an}} - \epsilon_{\text{mat}}}{\epsilon_{\text{an}} + 2\epsilon_{\text{mat}}} \tag{10}$$

In the equation, ϵ_{eff} is the effective dielectric function, ϵ_{mat} is the bulk material dielectric function, f is the analyte volume fraction,[33] and ϵ_{an} is the analyte dielectric function. This equation, which was designed to describe composite dielectric functions for mixtures, is most appropriate when one species dominates the bulk of the volume of mixture. This is the case for an analyte incorporated into a bulk matrix at relatively low concentrations. Maxwell−Garnett theory has been applied to many different types of composite systems, notably, metal-oxide/metallic nanoparticle composites,[34,35] monolayer-coated metallic films,[36] and silicon-air photonic crystals.[37]

In applying the analysis to the vapochromic lattice, the value employed for ϵ_{an} was the square of n_{CHCl_3} (=1.4459). The analyte was assumed to replace vacuum or dilute air ($\epsilon_{\text{air}} \approx n_{\text{air}}^2 \approx 1$) in the porous material's voids. We further assumed that ϵ_{mat} consisted only of a real component calculable from Kramers−Kronig theory and an imaginary component derived from the scaled absorption spectrum of the lattice material:

$$\epsilon_{\text{mat}} = [n_{\text{K-K}} + ik_{\text{abs}}]^2 \tag{11}$$

The volume fraction of analyte, f, used in the effective-medium calculation was 0.0215. This value, equivalent to the incorporation of 0.6 chloroform molecules per lattice formula unit, was determined via quartz crystal microbalance measurements (data not shown) and is consistent with previously reported values.[16]

(32) Garnett, J. C. M. *Philos. Trans. R. Soc. London* **1904**, *203*, 385.
(33) The volume fraction, *f*, is simply the volume occupied by the analyte divided by the total volume.
(34) Ung, T.; Liz-Marzan, L. M.; Mulvaney, P. *J. Phys. Chem. B* **2001**, *105*, 3441−3452.
(35) Harnyak, G. L.; Patrissi, C. J.; Martin, C. R. *J. Phys. Chem. B* **1996**, *100*, 1548−1555.
(36) Zeman, E. J.; Carron, K. T.; Schatz, G. C.; Van Duyne, R. P. *J. Chem. Phys.* **1987**, *87*, 4189−4200.
(37) DeDood, M. J. A.; Snoeks, E.; Moroz, A.; Polman, A. *Opt. Quantum Electron.* **2002**, *34*, 145159.

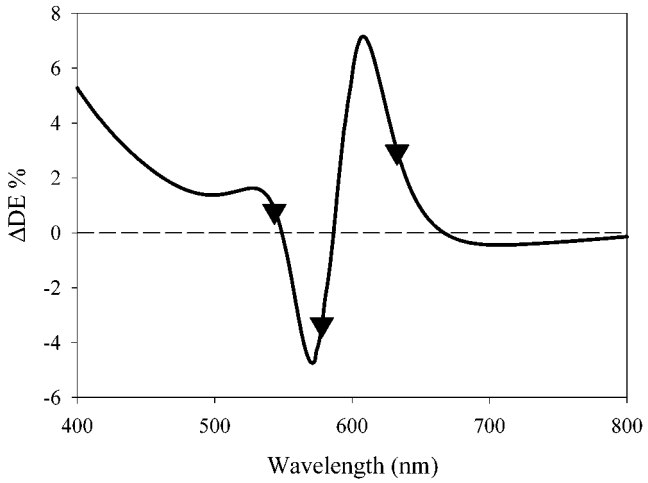

Figure 7. Wavelength-dependent diffraction response upon chloroform addition described by the complete theoretical description, involving consideration of the change in lattice refractive index as $\Delta(n + ik)$ and the inclusion of an effective-medium approximation of the intercalated analyte. Experimental data (▼) are plotted to illustrate the agreement with theoretical description.

Table 1. Comparison of Experimental and Theoretical Values for the Change in Diffraction Efficiency upon the Addition of 49 g/m^3 of $CHCl_3$

wavelength (nm)	experimental ΔDE %	theoretical ΔDE %
543.5	0.79 ± 0.01	0.80 ± 0.02
578	-3.34 ± 0.08	-3.38 ± 0.02
632.8	2.95 ± 0.03	2.96 ± 0.02

Having accounted for the presence of analyte, the percentage change in diffraction efficiency at the monitored spot ($I_{1,0}$) was modeled according to eq 6 (where again, because of the low absorbance of the chromophoric lattice, $\eta_{1,0}$ should be well approximated by the loss-corrected diffraction efficiency ($DE_{1,0}$) measured experimentally).

Needed values for ϕ were generated using input functions describing the complex index of refraction of the lattice material before and after $CHCl_3$ addition. In subsequently estimating the index contrast ($\Delta\tilde{n} = \tilde{n}_{mat} - \tilde{n}_{atmosphere}$), we assumed that $\tilde{n}_{atmosphere}$ was ca. 1 and that the addition of chloroform vapor did not significantly perturb its value. To simulate the system before $CHCl_3$ addition, an input function of the form $\tilde{n} = n_{K-K} + ik_{abs}$ was used. The square root of ϵ_{eff} was used to simulate the material after $CHCl_3$ addition. The adjusted ϕ functions were then used in eq 6 to calculate diffraction efficiencies.

The final results of the modeling, incorporating both Kramers−Kronig and effective-medium effects, are plotted as a function of wavelength in Figure 7. Additionally, the results at discrete wavelengths corresponding to experimental measurements are also listed in Table 1. Agreement with experiment is clearly very good and, indeed, would appear to be sufficient to calculate optimal probe wavelengths and predict amplification responses with good accuracy for other candidate analyte/lattice-material combinations, given electronic absorption spectra as input data.

Modeling Chemical Selectivity. In view of the remarkable difference in sensor signal size for chloroform versus methanol at $\lambda_p = 632.8$ nm, and the evident lack of resonant signal amplification for the latter, we extended the combined Kramers−Kronig/effective-medium approximation calculations to methanol. For simplicity, the volume fraction of methanol within the lattice under saturated vapor conditions was assumed to equal that found for chloroform.[38] The results of the full calculation are shown in Figure 8, with the corresponding results for chloroform plotted again for comparison. In agreement with experiment, the calculation indicates a very small change in diffraction efficiency at 632.8 nm upon exposure to methanol. Although we did not investigate this point experimentally (laser line unavailable), the calculations predict that at a probe wavelength of ∼565 nm the chemical selectivity will be reversed; amplification will be substantial for methanol uptake but absent for chloroform.

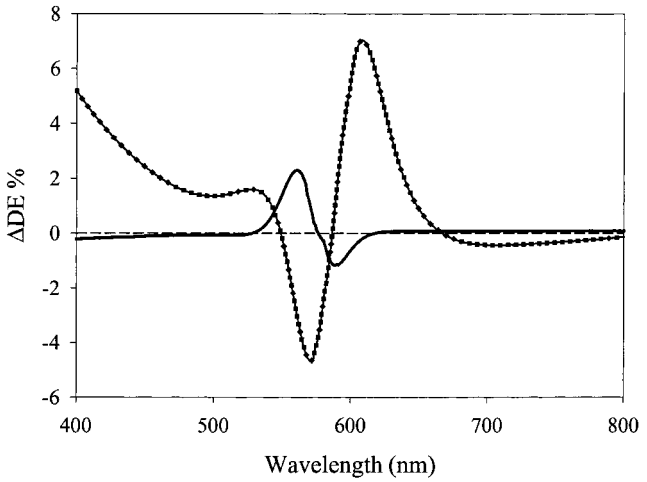

Figure 8. Calculated wavelength-dependent diffraction response of the [Pt($CNC_6H_4C_{10}H_{21}$)$_4$][Pd(CN)$_4$] diffraction grating upon methanol addition (−). The diffraction response for chloroform (−■−) is included for reference.

Analytical Implications. While chloroform does not present an enormous environmental or occupational health hazard, it is worth considering the analytical chemical implications of these initial studies (recognizing, of course, that more detailed studies will be required to draw rigorous conclusions). As evident from the data in Figure 4, the isotherm for chloroform uptake by the vapochromic salt is far from linear. Distinct thresholds exist at ca. 2 g/m^3 and 20−25 g/m^3, and an intrinsic sensitivity limitation exists, therefore, for this particular choice of lattice material. The existence of such thresholds is qualitatively consistent with independent observations, via quartz crystal microgravimetry, for similar materials, and their origin has recently been discussed in some detail.[39] In any case, the isotherm imposes a functional detection limit of a few g/m^3 upon the resonant sensing experiments for this particular analyte/lattice-material combination.

To place the findings in perspective, we note that severe immediate effects due to acute chloroform exposure (e.g., nervous system depression, altered rate of respiration, nausea, and vomiting) reportedly occur only at very high concentrations (∼1500 ppm), consistent with the known limited toxicity of chloroform.[40] Nevertheless, significant additional risks due to

(38) While we lack data to corroborate this assumption, it has been observed, for a related compound, that these two similarly sized analytes are taken up to similar extents under high vapor pressure conditions (six chloroform molecules and eight methanol molecules per salt unit).

(39) Grate, J. W.; Moore, L. K.; Janzen, D. E.; Veltkamp, D. J.; Kaganove, S.; Drew, S. M.; Mann, K. R. *Chem. Mater.* **2002**, *14*, 1058−1066.

(40) Data obtained via the United States Environmental Protection Agency Technology Transfer Network, see: http://www.epa.gov/ttn/uatw/hlthef/chlorofo.html.

chronic exposure exist and have led to exposure limits that are considerably lower. The threshold limit value (TLV) as set forth for chloroform by the American Conference of Governmental Industrial Hygenists (ACGIH) is 10 ppm, while the OSHA permissible exposure limit (PEL) and NIOSH recommended exposure limits (REL) are both ~2 ppm.[39] Notably, the reported human odor threshold (85−300 ppm)[39] is well above these levels, suggesting that artificial sensing could be of real value. With perhaps a 2- to 5-fold improvement in sensitivity, an analytical device based on the resonant diffraction scheme described here might well be suitable for environmental and human health monitoring applications.

Conclusions

Micropatterning of the vapochromic charge-transfer salt $[Pt(CNC_6H_4C_{10}H_{21})_4][Pd(CN)_4]$ on transparent platforms yielded structures that behave as transmissive two-dimensional visible-region diffraction gratings or "photonic lattices". These lattices have been investigated as volatile organic compound (VOC) sensors via a newly devised signal transduction scheme involving diffraction of visible light. We find that by monitoring changes in the diffraction efficiency at wavelengths resonant with an electronic transition, large amplifications of sensor signals can be observed (up to 3.5 orders of magnitude for the system examined here). The magnitude of the signal amplifications, as well as their signs, is strongly wavelength dependent. We find that both can be successfully computationally modeled for a test case involving chloroform vapor sensing. The modeling consisted of a Kramers−Kronig analysis that incorporated absorptivity effects and that explicitly accounted for dielectric effects, due to the incorporated analyte, via an effective-medium calculation. We are currently exploring additional examples of resonance amplification based on other types of materials (dye-containing polymeric materials and nanoscale metallic materials). We are also exploring array-based versions of the resonance-amplified sensing scheme with the objective of obtaining devices capable of determining, at least qualitatively, the identities of *unknown* analytes at very low concentrations.

Acknowledgment. We thank Prof. George Schatz, Aaron Massari, Dr. Keith Walters, Dr. Jay Grate, and Prof. Kent Mann for helpful discussions. This work was supported by the MRSEC program of the National Science Foundation (DMR-0076097) at the Materials Research Center of Northwestern University and by NSF grant no. CHE-9810483.

JA0177354